Structural Chemistry (2023) 34:399–412
https://doi.org/10.1007/s11224-022-01983-3

ORIGINAL RESEARCH

Novel *pull–push* organic switches with D–π–A structural designs: computational design of star shape organic materials

Abrar U. Hassan[1] · Ayesha Mohyuddin[2] · Cihat Güleryüz[3,4] · Sohail Nadeem[2] · Nyiang K. Nkungli[5] · Sadaf U. Hassan[2] · Mohsin Javed[2]

Received: 14 February 2022 / Accepted: 31 May 2022 / Published online: 17 June 2022

Abstract

The structural alteration with π-linkers was used to design a donor–acceptor type series of 2,2′-(pyrimidine-4,6-diyl)bis(2,3-dihydro-1,3-benzothiazole) (**PB**)-based chromophores (**AH1**–**AH7**) to exploit the adjustments in their optical characteristics. To investigate the electronic geometries, absorption wavelengths, charge transfer processes, and the effect of structural alterations on nonlinear optical (NLO) characteristics, density functional theory (DFT) simulations have been used. During the UV–visible study, several long-range and range separated functionals like B3LYP, CAM-B3LYP, B97XD, and APFD with the 6-311G + (d,p) basis set were used to select the efficient level at DFT. As a response, UV–vis data indicated an intriguing consistency at the B3LYP level across experimental and TD-DFT-based values of **PB**. All the designed molecules had a smaller energy band gap (0.84–3.67 eV) and wide absorption spectra inside the visible region. Natural bond orbital (NBO) results indicated a significant push–pull operation, with donors and π-conjugates exhibiting positive values and most acceptors exhibiting the minimum values. Electronic transformations between electron donors to acceptor moiety, Trifluoromethyl (**TFM**) via π-conjugated linkers were shown to have a superior linear $<\alpha>$ and nonlinear (β_{total}) NLO values of 306–474 and 40–230 Debye-Angstrom^{-1} respectively. When chromophores with one phenyl π-linker were compared to those with the two π-linkers, the chromophores with the higher π-linker showed increased hyperpolarizability. The highest second-order hyperpolarizability (β) was found to be 230.11 Debye-Angstrom^{-1} which was about five times higher than urea (standard). This research has shown that by manipulating the kind of π-spacers, novel metal-free NLO compounds may be created, which might be used for high-tech NLO purposes.

Keywords Structural alteration · Nonlinear optical materials · NBO · Hyperpolarizability · Density functional theory

Introduction

Molecular substitution-oriented designing is a novel strategy for developing new materials with new properties [1]. The technique might be expanded to the finding of high-performance ultraviolet (UV) nonlinear optical (NLO) solid-state materials by carefully adjusting the replacement atoms [2]. Organic materials (OMs) are utilized in a variety of semiconductor devices due to their high charge transportation with photo-adjustable characteristics [3]. These OMs find a wide range of possibilities in semiconductor devices such as energy conversion [4], optoelectronics [5], and photovoltaics [6]. They have recently created numerous technologies inside Organic Light-Emitting Diodes (OLEDs) [7], as well as organic field-effect transistors (OFETs) [8]. Because of their multi-purpose uses, OMs are a subject of research for synthetic specialists as well as scientific theorists [9]. Organic-based π-conjugated compounds as semiconductors also have promising uses in optoelectronics [10]. The most recent research on π-conjugated acenes and hydrocarbons has rapidly expanded their use in the electronics sector [11]. It is critical to generate tunable organic substituents with improved mobility and stability [12]. At the present,

✉ Abrar U. Hassan
hassanabrar2016@gmail.com

[1] Department of Chemistry, University of Gujrat, University of Gujrat, Gujrat 54400, PK, Pakistan

[2] Department of Chemistry, University of Management and Technology Lahore, Johar Town, Lahore, Punjab C-II, Pk, Pakistan

[3] Department of Physics, Marmara University, Ziverbey, Istanbul 34722, Turkey

[4] Department of Opticianry, Altınbaş University, 34144 Istanbul, Turkey

[5] Department of Chemistry, Faculty of Science, The University of Bamenda, P.O. Box 39, Bambili-Bamenda, Cameroon

quantum chemical techniques are being used to reveal different characteristics of interest [13]. Various structural changes are well-planned as an unrivalled strategy for tuning the optical and charge transport characteristics of organic semiconductor materials (OSMs) [14]. To analyze their properties, the energy of molecular orbitals (E_{HOMO} and E_{LUMO}, etc.), electron affinities (EA), ionization energies (*IE*), and relevant global chemical reactivity properties have been investigated. Density functional techniques have advanced, and they now have the first-rate predictive capability for calculating charge transport and electro-optical characteristics [15].

Nonlinear optical (NLO) materials have been acknowledged to interface with light to generate a nonlinear behavior and their organic/inorganic composition. Nonlinear optical (NLO) materials hold the potential to play a function in processing applications, fibre optics, telecommunications, and information management [16]. Nonlinear optics has become increasingly significant in current optical fibre networking systems enabling ultrafast processing applications [17]. Nonlinear dynamics have both positive and/or negative side effects for light travelling via an optical cable. Due to various relatively simple reaction chemistry, cheap cost creation, and structurally feasible alterations to allow for a distinct NLO response, NLO compounds produced from the organic framework became the topic of recent research [18]. Optical devices such as lenses, reflectors, prisms, polarizing filters, sensors, and modulators may bend, refract, broadcast, disperse, polarize, monitor, and change light [19]. The intramolecular charge transfer (ICT) across charge transfer components through π-conjugated linkers underpins these NLO properties of materials [20]. Computational and experimental results suggest that building robust donor (D) and acceptor (A) groups on opposing sides of π-linkers can result in a wide second-order NLO responding [21]. Electronic charge transitions are accelerated in compounds containing conjugated π-electrons [22]. The molecular electrostatic potential (MEP) is a useful measure for studying the reactivity of various molecules and/or species [23].

Since expensive synthetic procedures have hampered the advancement of UV laser technologies, new strategies for developing superior UV NLO materials are critically needed [24]. Transfer of inter/intramolecular charges, concerning both the electron donors and the withdrawing group [25], can be used to optimize the bandgap and govern transitions in a novel donor–acceptor system employing various donor or acceptor moieties with large initial dipole moment values [26]. The electronic characteristics of **D–π–A** organization with the novel π-conjugated network are introduced in the system consisting of 2,2′-(pyrimidine-4,6-diyl)bis(1,3-benzothiazole) (**PB**) with conjugates benzenes serving as second π-linkers between the donor and acceptor moieties. TFM has been employed in many hole-transporting materials as a donor unit because of its potential for electron donation and charge transfer [27]. Seven newly designed PB–TFM-based dyes (**AH1—AH7)** of D—π—A type have been created with varied combinations of first and second π-conjugates. Such theoretical evaluation helps estimate NLO attributes as well as investigate the influence of various π-conjugated linkers on this activity without any expense. The newly developed dyes (**AH1—AH7**) were computed using density functional theory (DFT) for their electronic properties, electronic features, and polarizability/hyperpolarizabilities (Scheme 1). This study should hopefully lead to the development of novel organic dyes to exhibit good NLO characteristics.

Computational methodology

The standard research design was carried out to investigate the structural, electronic and quantum chemical characteristics [28]. PB–TFMs derived new dyes at their ground state geometry (S_0) had been optimized using Becke's three-parameter hybrid (B3LYP) and the 6-31G + (d,p) basis set at the density functional theory level. Different long-range and range separated functionals, B3LYP, CAM-B3LYP, B97XD, and APFD, were investigated using the 6-311G + (d,p) basis set at density functional theory (DFT) level for PB at its UV–vis studies. The absorption spectra of TDDFT-based findings were found to match with experimental data at the B3LYP level. Although the B3LYP functional employed for TD-DFT calculations does not compensate for long-range interactions, the theoretical and experimental [29] UV–vis spectra were in good agreement, demonstrating that the functional was suitable in this context (Fig. 1). The B3LYP model, which contains Hartree–Fock exchange, local exchange, gradient exchange adjustment, local correlation, and gradient correlation correction, is the most well-known hybrid density functional theory model [30]. The basis sets of 6-311G + (d,p) are frequently used in conjunction with B3LYP and are recommended when hydrogen plays a significant role [31]. It does not consider dispersion effects and lacks polarization functions. At ground state (S_0) optimization, the conventional DFT functional (B3LYP) has offered the best justification for geometry optimizations at their energy minima [32]. Time-dependent density functional theory (TD-DFT) calculations were employed to calculate the absorption spectra of newly designed dyes at the same basis set level using the B3LYP functional. TD-DFT calculations are still proved to be an efficient approach for calculating the various electronic (absorption, emission and dipole moment, etc.) features of molecules [33] which play a critical role in their charge transferability [34]. In the majority, coupling activities were aided by their increased charge mobility [35], which might be inhibited by organic-organic contacts [36], when contrasted

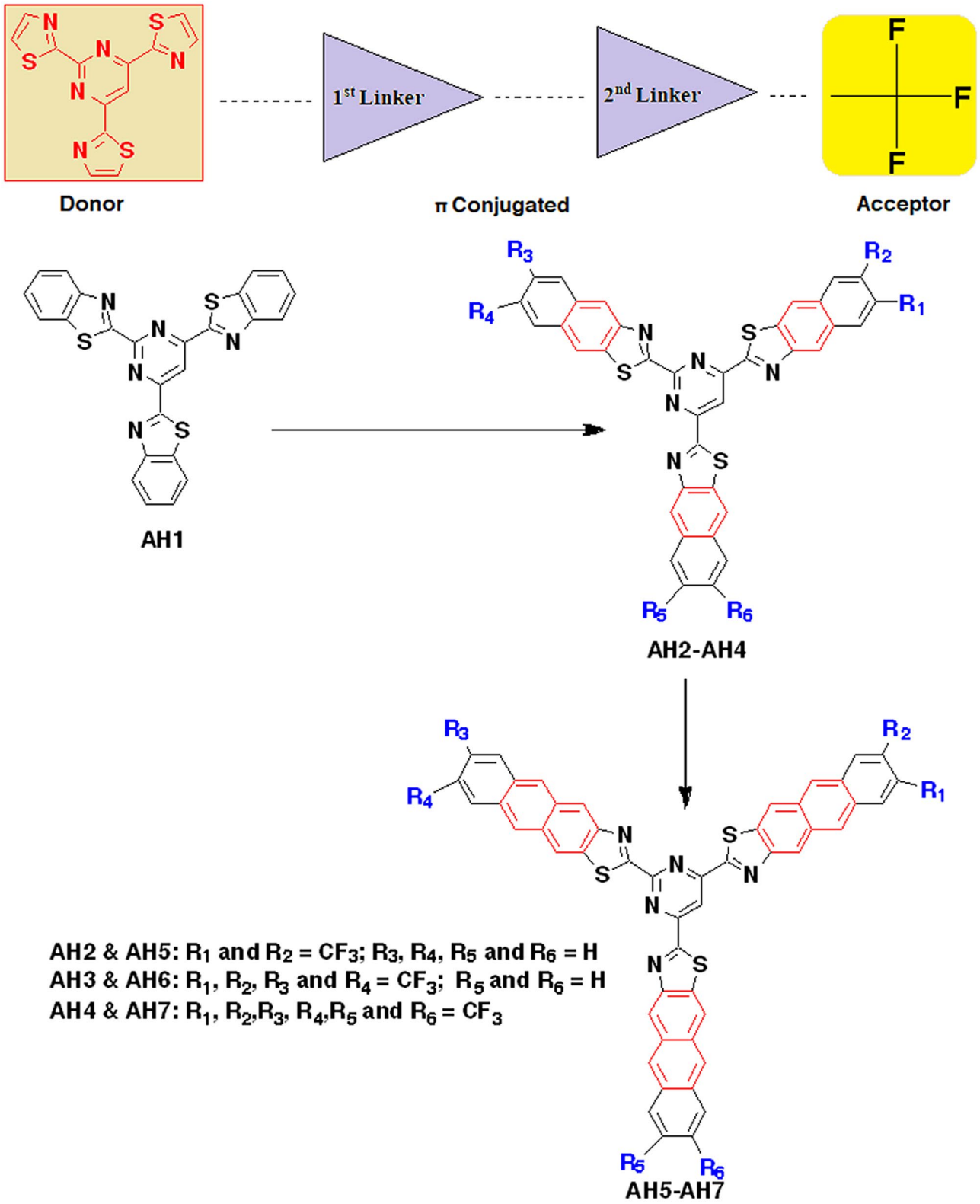

Scheme 1 Structural design of compounds (AH1–AH7) with the acceptor, linkers, and donor designs

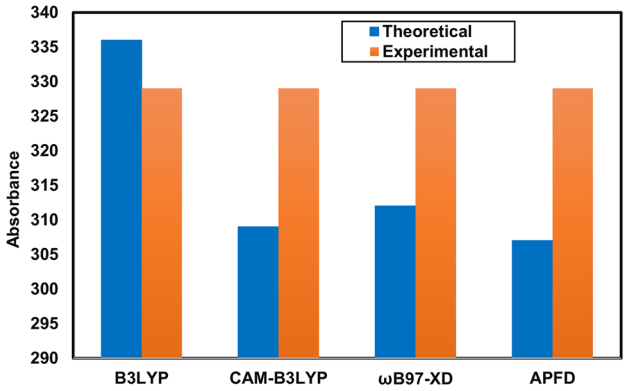

Fig. 1 UV–vis benchmark study of **PB** at B3LYP, CAM-B3LYP, B97XD, and APFD with the 6-311G+(d,p) to simulate its experimental result

to polaron-localized relaxation energy when examining individual entities [37].

The polarizability, as well as hyperpolarizability tensors of the designed dyes, was calculated using Eqs. (1) and (2).

$$< a >= 1/3(a_{xx} + a_{yy} + a_{zz}) \tag{1}$$

Similarly, second-order hyperpolarizability (β) are computed as follows:

$$\beta_{\text{tot}} = \left[\left(\beta_{\text{xxx}} + \beta_{\text{xyy}} + \beta_{\text{xzz}}\right)^2 + \left(\beta_{\text{yyy}} + \beta_{\text{xxy}} + \beta_{\text{yzz}}\right)^2 + \left(\beta_{\text{zzz}} + \beta_{\text{xxz}} + \beta_{\text{yyz}}\right)^2 \right]^{1/2} \tag{2}$$

Light-harvesting efficiency (LHE) is another crucial component that affects optical performance. The compounds with the highest photocurrent responsiveness are those with a high LHE value [38]. Equation (3) was used to calculate the LHE of newly designed chromophores.

$$LHE = 1 - 10^{-f} \tag{3}$$

The oscillator strength of substances is represented by "f" in the preceding equation [39]. As an unparalleled technique for tweaking the optical and charge conduction properties of organic semiconductors, different structural alterations are well (Eq. (4)).

$$\beta_{CT} = \frac{\Delta\mu_{gm} f_{gm}}{E_{gm}^3} \tag{4}$$

The difference between excited to ground states is defined by E_{gm} [40], and the dipole moment is proportional to hyperpolarizabilities. The oscillator strength from a ground state to the n_{th} excited state (f_{gm}) is proportional to β, while E^3_{gm}, the transition energy inside the cube, is contrariwise related to β [41].

All the global chemical reactivity parameters were calculated by utilizing the Koopmans theorem [42]. By the Eqs. (5) and (6)

$$\boldsymbol{IP} = -E_{HOMO} \tag{5}$$

$$\boldsymbol{EA} = -E_{LUMO} \tag{6}$$

The chemical potential ($\boldsymbol{\mu}$) of a molecular system is related to the following equation:

$$\boldsymbol{\mu} = -\left(\frac{\boldsymbol{IE} + \boldsymbol{EA}}{2}\right) \tag{7}$$

Hardness ($\boldsymbol{\eta}$) and softness ($\boldsymbol{\sigma}$) of a molecular system are also very important global reactivity parameters which are computed as follows:

$$\boldsymbol{\eta} = \frac{1}{2}[\text{H-L}] \tag{8}$$

$$\sigma = \frac{1}{2\eta} \tag{9}$$

$$\boldsymbol{x} = \left(\frac{\boldsymbol{IE} + \boldsymbol{EA}}{2}\right) \tag{10}$$

$$\boldsymbol{\omega} = \left(\frac{\boldsymbol{\mu}^2}{2\boldsymbol{\eta}}\right) \tag{11}$$

The NBO analysis sought to learn more about the charge transfer (CT) from the donor to such acceptor [43]. The title dyes with their stabilization energy were calculated at their second-order perturbations theory analysis.

$$E^{(2)} = \mathrm{q_i}\frac{\left(\mathrm{F_{i,j}}\right)^2}{\varepsilon_\mathrm{j} - \varepsilon_\mathrm{i}} \tag{12}$$

Results and discussion

Structural optimization of modulated D–π–A systems

For donor–linker–acceptor type dyes, screening the π-spacers is critical for achieving a good NLO performance. The goal of this study is to create a new 2,2′-(pyrimidine-4,6-diyl)bis(2,3-dihydro-1,3-benzothiazole)-based potential NLO materials by structural customization with different -bridges and to forecast their photoluminescence, electrical, and NLO characteristics for the modern optoelectronics. A

synthetic metal-free heterocyclic PB is employed in this study for theoretical design. Four optimized structures (**AH1**–**AH4**) are given in Figs. 1 and 2 as representative structures while all other structures are elaborated in the Supplementary Information (Tables S1–S7) Our dyes are made up of three primary components: (i) 2,2′-(pyrimidine-4,6-diyl)bis(2,3-dihydro-1,3-benzothiazole) (**PB**) as a donor moiety, (ii) the first and second π-spacers (phenyl), which together served as a bridge, and (iii) Trifluoromethyl (**TFM**) as the acceptor moiety. Two phenyl-conjugates were used to create a total of 7 dyes with altering acceptor atoms. In all studied compounds, the dihedral angle involving C–C–C in the benzene ring of the PB molecule was determined to be 117.65°–118.09° (**AH1–AH7**). C–C–N connected bond angles were discovered to be 106° and 110°, respectively. At 112.43°–113.03°, the lateral benzene ring was observed to be comparable. The benzene ring C–C–C of benzyl facing thiazole had a 120° dihedral angle, whereas the TPA side had a 108° geometric angular position. C–C–N in the pyrrole unit and C–N–N in the thiazole unit have dihedral angles of 106.43°–106.65° and 110.34°–110.39°, correspondingly.

For the research of NLO attributes, DFT and TD-DFT calculations are used to evaluate electronic oscillations, (and tot), NBO analysis, and spectrum absorption analysis, as well as light-harvesting efficiency (LHE).

Electronic and global reactivity features

FMOs analysis is a valuable tool for determining the stabilities and photovoltaic characteristics of compounds [44]. The FMOs, or the highest occupied molecular orbital (HOMO) or the lowest unoccupied molecular

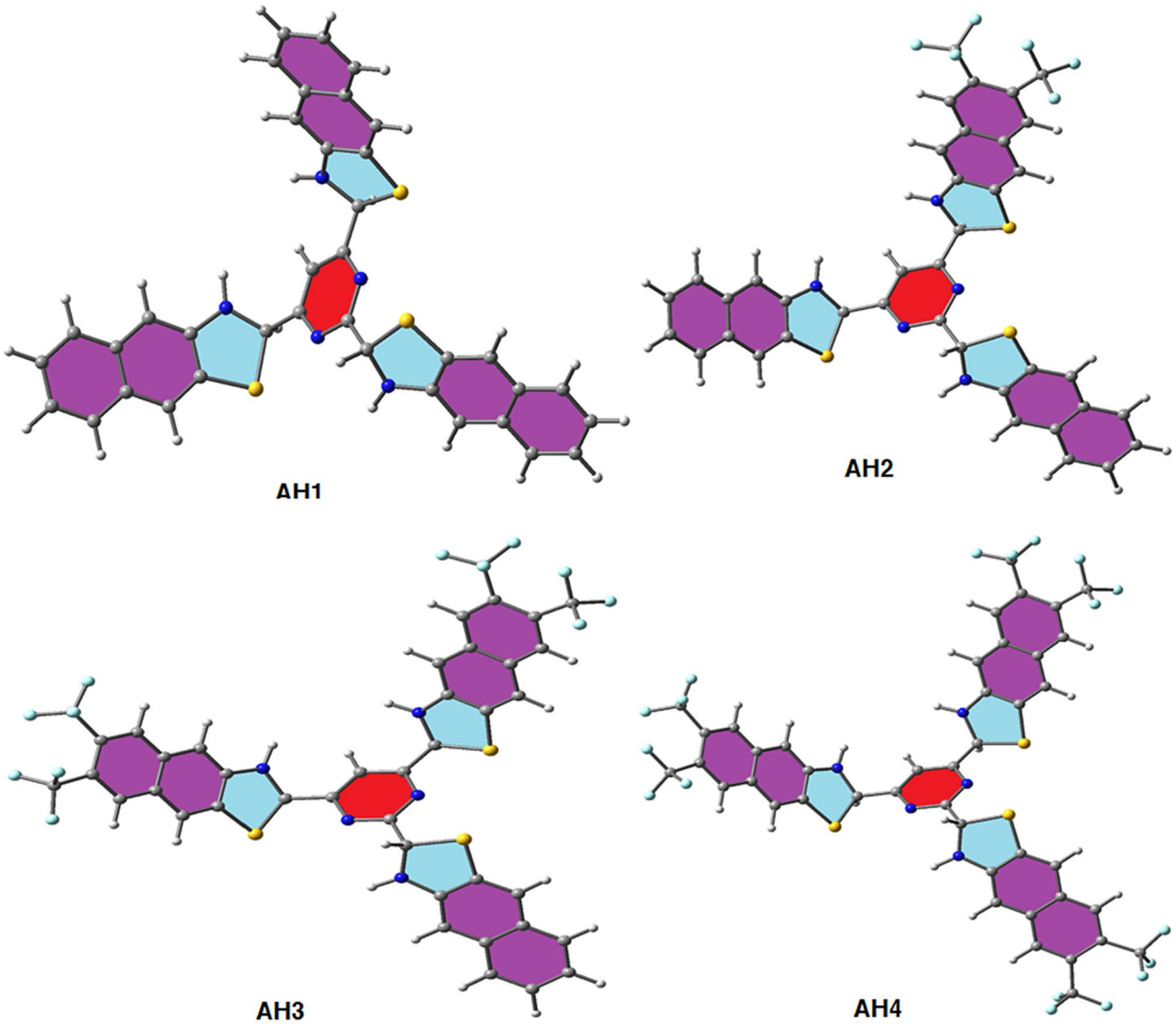

Fig. 2 Optimized structures of representative compounds (**AH1–AH4**) at the DFT level

orbital (LUMO), are important in optical absorption for mechanical simulation of substances [45] (Fig. 3). The bandgap (E_{LUMO}–E_{HOMO}) is the most important element in determining the stability and chemical reactivity of novel compounds (**AH1–AH7**) [46]. Enhanced HOMO–LUMO design for a molecule is associated with its low reactivity, more stability, as well as a hard molecule, whereas smaller E_{LUMO}–E_{HOMO} energy gaps are associated with more reactivity, lesser stability, and *softer* molecules which are more polarized and start serving as a finer competing product in offering the best NLO response. The bandgap across the molecular orbitals was calculated to utilize its significance for their promising photophysical characteristics. Table 1 shows that **AH4** having the first π-conjugated link with the highest number of **TFMs** had the smallest bandgap (0.84 eV) among all. Additionally, **AH5** and **AH6** which had two π-spacers and 2 and 3 acceptor TFMs respectively were more sensitive after **AH4**. The rising bandgap ordering of such dyes revealed that **TFMs** had delivered the best results with phenyl spacers to reduce the energy gap. 0.84–3.67 eV. It was also discovered that dyes containing more π-spacers had a narrower bandgap and therefore stabilizing the molecule more. Overall, the maximum energy gap was found in **AH3** (3.67 eV), while the lowest bandgap found in **AH4** was 0.84 eV. The energy band gap of all analyzed dyes is evaluated in the following order: **AH4** (0.84) > **AH6** (1.35) > **AH7** (2.35) > **AH1** (2.43) > **AH5** (2.86) > **AH2** (2.97) > **AH3** (3.67). In specific, the charge concentrations on the surface of orbitals were studied and depicted in Fig. 3. The charge distributions in HOMOs were distributed throughout the molecule, whereas in LUMO, they are distributed mostly at accepter moiety and partially across the pi spacers.

By examining the global reactivity parameters (GRP) [47] comprising such ionization potential (IP), electron affinity (EA), electronegativity (x), global hardness (η), chemical potential (μ), global electrophilicity (ω), and global softness (σ), the E_{LUMO}–E_{HOMO} has been used to depict reactivity and stability. The results for the examined dyes were computed from their molecular orbital analysis by utilizing proper quantum chemistry implications. Ionization potential, as well as electron affinity amplitudes, were used to determine a compound with its electron-donating and electron-accepting capacities respectively [48]. The ionization potential (IP) represents the energy necessary to liberate one electron from that molecule. Increased IP values suggest greater chemical resistance to oxidation and stability. **AH6** had the highest IP value of 7.02 eV, while **AH4** had the lowest value of 0.89 eV. Their overall order was found as follows: **AH6** (7.02) > **AH3** (3.78) > **AH2** (3.24) > **AH1** (2.97) > **AH5** (2.94) > **AH7** (2.84) > **AH4** (0.89). Furthermore, **AH6** also had the highest EA value of 5.67 eV, while AH4 had a value of just 0.05 eV. The overall order was noted as follows: **AH6** (5.67) > **AH1** (0.54) > **AH7** (0.49) > **AH2** (0.27) > **AH3** (0.11) > **AH5** (0.08) > **AH4** (0.05). The IP values were found to be much higher than the EA values, implying that the proposed compounds had outstanding electron-accepting capacity. Chemical potential values ($\boldsymbol{\mu}$) are considered while determining the stability of compounds. This is related to molecule electronegativity; wherein low values indicate an easy acceptance of electrons and explain electron attraction. Overall order of all the dyes was found as follows: **AH4** (−0.47) > **AH5** (−1.51) > **AH7** (−1.66) > **AH1** (−1.76) > **AH2** (−1.76) > **AH3** (−1.94) > **AH6** (−6.35). The greater hardness values in the investigated dyes imply their stability, as evidenced by their negative chemical potentials. The rising energy gap sequence of entitled dyes corresponds to the ascending order for their global hardness. This design was in perfect agreement with the HOMO–LUMO bridging, illustrating that compounds with a significant E_g value are considered hard molecules, with greater kinetic stability, lower reactivity, and resistance against electronic conformation change. Overall order was noted as follows: **AH7** (1.84) > **AH5** (1.49) > **AH2** (1.43) > **AH4** (1.22) > **AH6** (1.17) > **AH3** (0.68) > **AH1** (0.42). Another factor to consider is global *softness*, which is connected to its chemical potential. The rising ordering of softness values was in a complete reversal of the growing energy gap order, displaying **AH2** (0.27) as the weakest reactive component with the lowest softness value; meanwhile, **AH4** (1.19) is the most reactive molecule with the greatest softness value as shown in their order: **AH4** (1.19) > **AH3** (0.74) > **AH1** (0.43) > **AH7** (0.41) > **AH6** (0.35) > **AH5** (0.34) > **AH2** (0.27). Global reactivity descriptors exhibited a high association with HOMO–LUMO band gap order (Table S4).

UV–visible analysis

Computed Ultraviolet–Visible (UV–visible) spectroscopy at TD-DFT level with B3LYP/6–311 + G (d, p) basis sets was investigated using DFT simulations. The lowest singlet–singlet six energy transformations were investigated during TD-DFT calculations (Fig. 4). Table 5 shows the calculated transition energy (E_{ge}), oscillator strength (f_{os}), the character of transitions, and optimum absorption wavelengths ($\boldsymbol{\lambda}_{max}$), whereas Fig. 2 shows the spectra of **AH1**–**AH7**. In general, all the dyes demonstrated the UV–visible absorbance span. The greatest value for $\boldsymbol{\lambda}_{max}$ is investigated in **AH3** for all compounds with one pi-spacer (436 nm) and two **TFM**s. As the π-linker increased, the maximum absorption value dropped, with the lowest value being 369 nm found in **AH5**. All the dyes were appeared to be in their descending order as follows: **AH3** > **AH1** > **AH4** > **AH2** > **AH6** > **AH7** > **AH5** (Table 2). The majority of electronic shifts (HOMO → LUMO) occurred between the donor (**PB**)

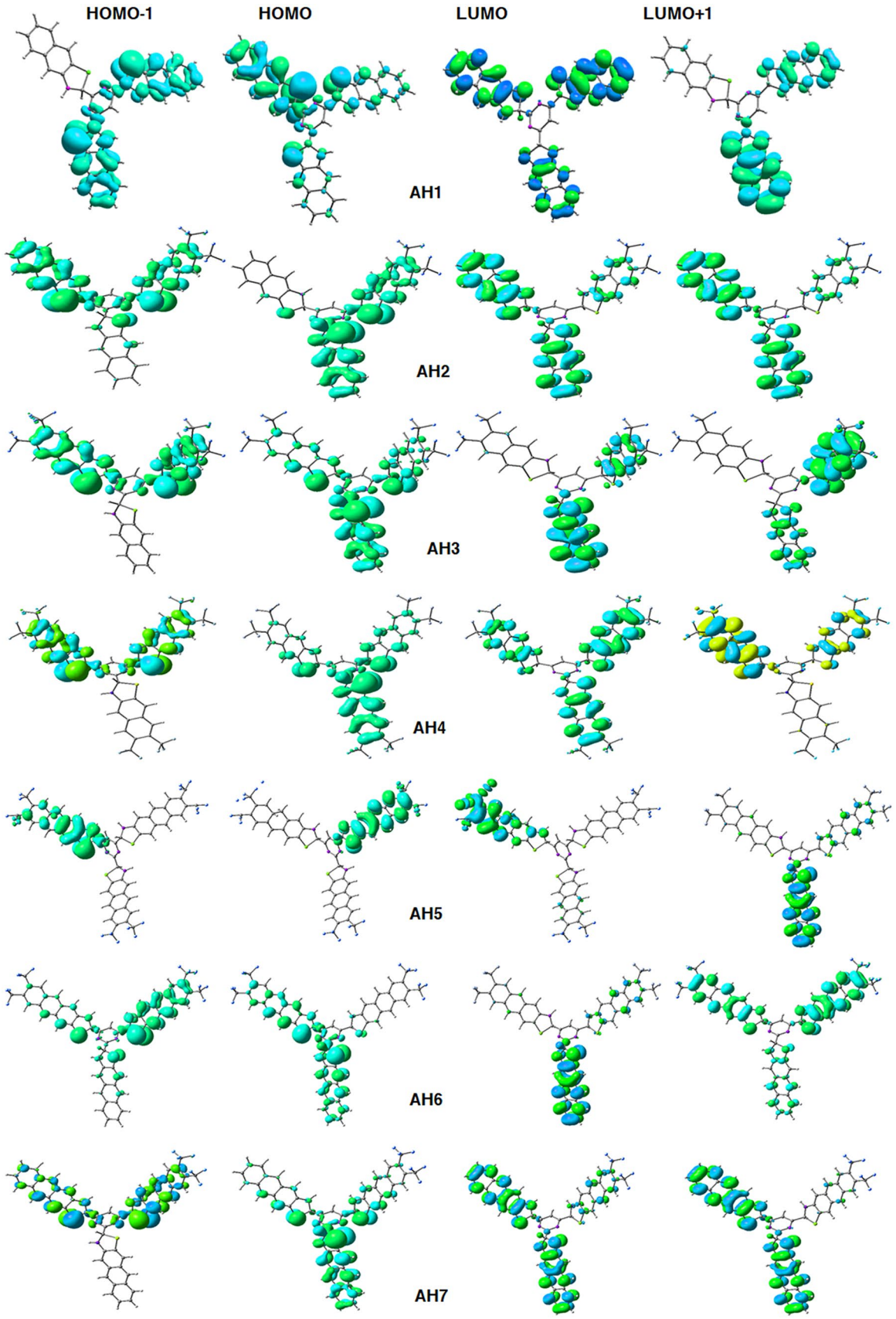

Fig. 3 Frontier molecular orbitals of new dyes (**AH1–AH7**) at their H-1, H, L, and L + 1 orbital levels

Table 1 Frontier molecular orbital energies (E_{HOMO} and E_{LUMO}), their energy gaps ($\Delta E_{HOMO-LUMO}$), and their related global reactivity parameter values

Parameter	AH1	AH2	AH3	AH4	AH5	AH6	AH7
E_{HOMO}	−2.97	−3.24	−3.78	−2.94	−0.89	−7.02	−2.84
E_{LUMO}	−0.54	−0.27	−0.11	−0.08	−0.05	−5.67	−0.49
$\Delta E_{HOMO-LUMO}$	2.43	2.97	3.67	2.86	0.84	1.35	2.35
(IP)	2.97	3.24	3.78	2.94	0.89	7.02	2.84
(EA)	0.54	0.27	0.11	0.08	0.05	5.67	0.49
Electronegativity (χ)	1.76	1.76	1.94	1.51	0.47	6.35	1.66
Potential (μ)	−1.76	−1.76	−1.94	−1.51	−0.47	−6.35	−1.66
Hardness (η)	1.22	1.49	1.84	1.43	0.42	0.68	1.17
Softness (σ)	0.41	0.34	0.27	0.35	1.19	0.74	0.43
Electrophilicity index (ω)	1.27	1.04	1.03	0.8	0.27	29.82	1.17

and the acceptor (**TFM**). The transition in **AH2** and **AH4** differed from the complete sequence of these dyes in which the transitions occur from HOMO-1 LUMO HOMO → LUMO + 3 respectively. The investigation of materials that harvest photons of solar light are known as light-harvesting [49]. This encompasses research into the light-harvesting characteristics of photosynthetic systems as well as artificial devices created to enhance photocatalytic processes or generate photovoltaic fuels [50]. In Table 5, the light-harvesting efficiency (**LHE**) values (Table 2) for the dyes **AH1**–**AH7** are shown. The

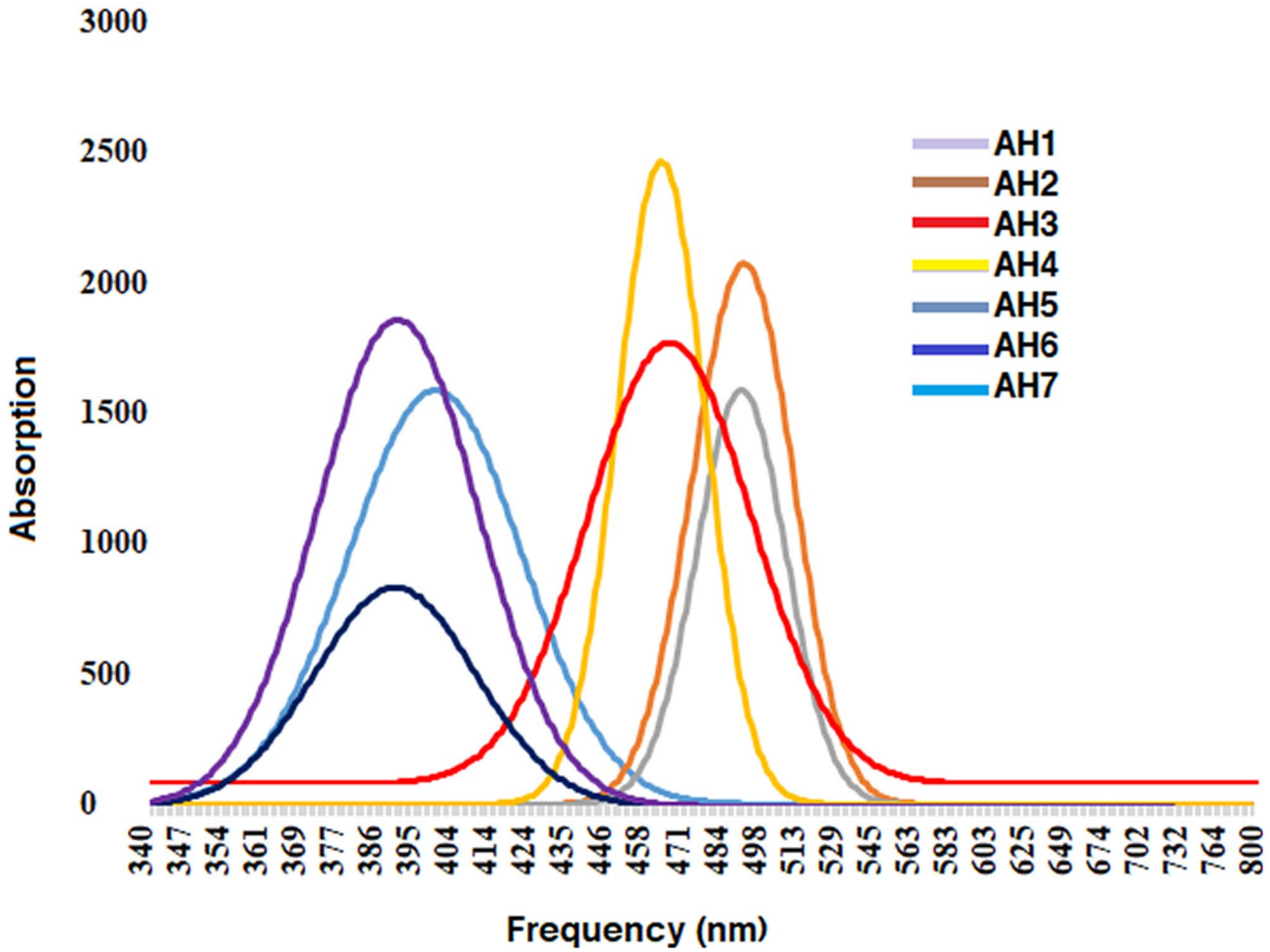

Fig. 4 UV–visible analysis of new dyes (**AH1–AH7**) at the DFT level

Table 2 Excitation energies (E_g), maximum absorption (λ_{max}), light-harvesting efficiency (LHE), and major electronic transitions of novel compounds

Comp	E_g	λ_{max}	f_{os}	*LHE*	μ_{gm}	Major transition
AH1	3.005	412	0.0071	0.02	5.3651	HOMO → LUMO (93%)
AH2	3.043	407	0.0141	0.03	5.9717	HOMO → LUMO + 1 (92%)
AH3	2.837	436	0.0004	0.00	5.4522	HOMO → LUMO (81%)
AH4	3.016	411	0.0058	0.01	8.0999	HOMO → LUMO + 3 (34%)
AH5	3.131	366	0.0119	0.03	6.9304	HOMO → LUMO (87%)
AH6	3.239	377	0.0108	0.02	3.6553	HOMO → LUMO (66%)
AH7	3.363	369	0.0188	0.04	4.2746	HOMO → LUMO (56%)

dye **AH7** had the highest LHE value of 0.04, which is the highest across all compounds.

Nonlinear optical parameters

The idea that lower HOMO–LUMO gaps boost the NLO behavior is well acknowledged [51]. This assertion holds in our researched systems, which offer significant promise for the prospective use of explored compounds in optoelectronic applications due to their robust NLO response. Table 3 shows that the highest is found in **AH1** (−276.09 Debye) which contains a π-linker and no acceptor, then reduces to **AH2** (−306.83 Debye), which contains a π-conjugated linker with one acceptor **TFM**; furthermore, it decreases to −474.48 Debye in **AH5**. The overall order was noted as follows: **AH1 > AH2 > AH7 > AH3 > AH4 > AH6 > AH5.**

A classical two model approach proposed by Oudar and Chemla [52] with the TD-DFT/6–31 G + (d,p) basis sets may be used to undertake a more extensive investigation of hyperpolarizability. The product of the two (or SOS) approach is used to implement a two-level model and it is widely used in the literature to study the NLO response [53]. It is calculated as follows:

$$\boldsymbol{\beta_{total}} = \frac{\Delta\mu X f_0}{\Delta E^3}$$

Table 3 First-order polarizability $\langle\alpha\rangle$ vales (Debye-Angstrom.$^{-1}$) of compounds with their tensors

Compounds	α_{xx}	α_{yy}	α_{zz}	$\langle\alpha\rangle$
AH1	−276.0663	−275.4510	−276.7602	−276.09
AH2	−331.1734	−308.8074	−280.5131	−306.83
AH3	−421.1916	−342.9182	−313.4685	−359.19
AH4	−429.4419	−410.8711	−351.5574	−397.29
AH5	−483.8467	−503.3657	−436.2138	−474.48
AH6	−503.7742	−441.1295	−386.1961	−443.70
AH7	−345.4901	−336.9281	−310.8316	−331.08

It contains the critical excited and ground state expressions with the polarizability description. The transition moments [54] and oscillation strengths are important components and NLO materials, with large transition moment and oscillator strength and low energy CT have demonstrated high values [55] (Fig. 5). The excitation wavelength is a significant feature in hyperpolarizability, where it is now being explored in various already reported excessive electronic systems.

The highest $\boldsymbol{\beta}_{tot}$ value 230.11 Debye-Angstrom^{-1} **AH5** was identified which had two π-linkers with one acceptor TFM (Table 4). The remaining compounds also showed good agreement with previously published Thiophene [56, 57] and thiazole-based [58, 59] relevant compounds. These findings show that the compounds studied, particularly **AH5** have had the potential to be employed as NLO candidates. Figure 4 depicts the good match between hyperpolarizability and thus the two-level approach for investigated molecules. **AH5 > AH4 > AH 6 > AH7 > AH1 > AH3 > AH2**. All the compounds had outstanding hyperpolarizability scores, indicating that structural alteration using efficient π-conjugated linkers in between donor and acceptor units is a successful approach for obtaining a pleasing NLO response. According to the foregoing conclusions, altering various types of bridges provides a critical notion in the modelling of unique D–A frameworks, resulting in outstanding NLO outcomes that can improve photoelectric as well as optical qualities.

Natural bond orbitals

Analysis of natural bond orbitals (NBOs) provides a very effective indicator for charge transfer relationships involving empty and filled orbitals [60]. It is often accepted that in processes, charge transfer is shifted from donors to the accepters over the molecular systems [61]. As a result, NBO analysis was carried out to better understand the charge transfer processes of our proposed compounds. This research revealed that all donor moieties had favourable charge transfer values, indicating that our developed compounds had a high potential for donation (Table 5). Furthermore, the very lowest (0.39–0.98 kcal/mol) NBO

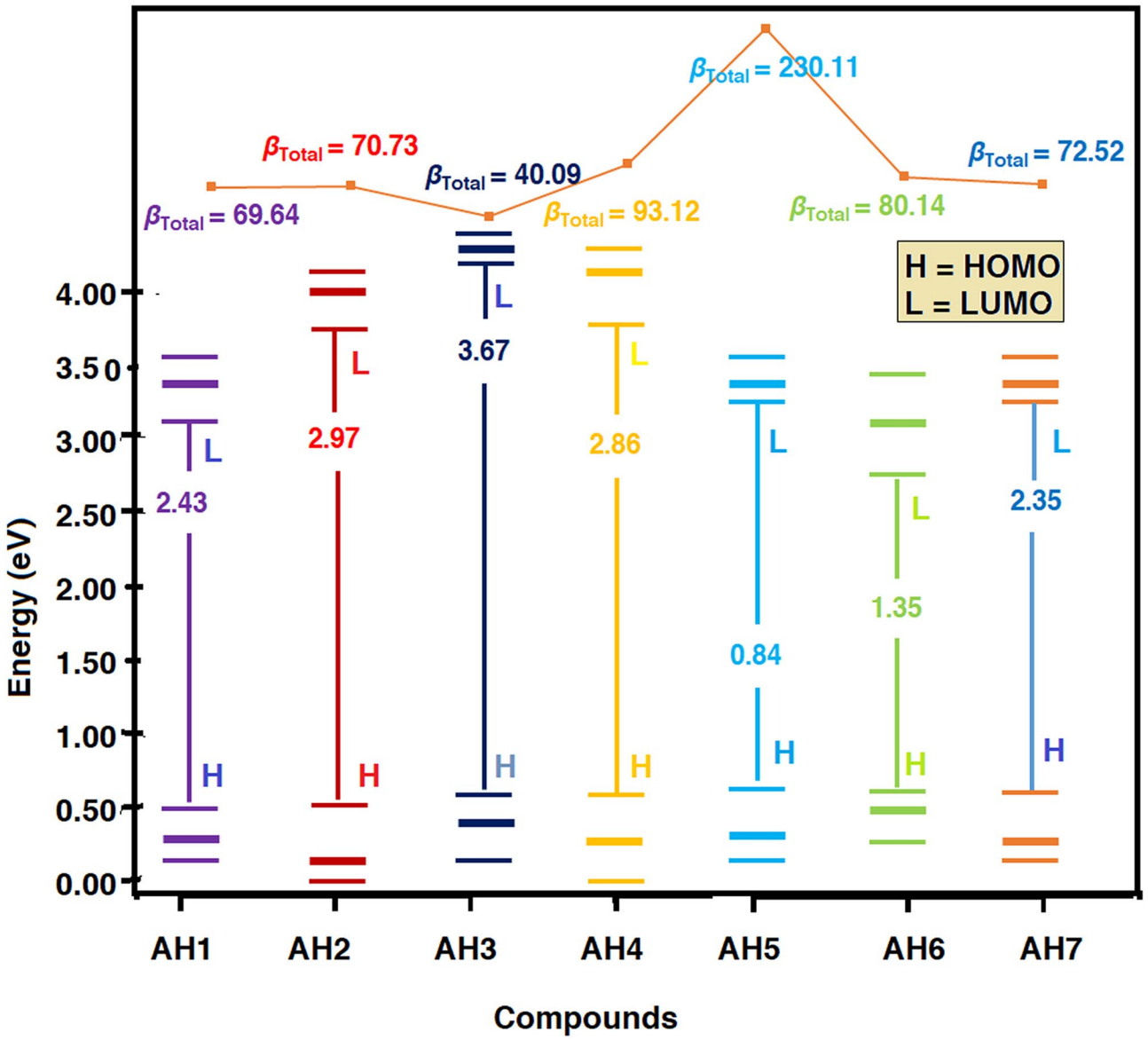

Fig. 5 Molecular orbitals, their energy gaps, and their hyperpolarizability values

energies of all acceptors demonstrated that all dyes can efficiently take electrons. The charge dispensation across the π-linkers revealed that they provide a pathway for electronic transfers. Overall, the investigation found that charge is successfully moved from donor to accept or via pi-spacers, resulting in a charge segregation state in which all donor and π-conjugated bridging display good ratings while all acceptors exhibit smaller values. The compound **AH7** with

Table 4 First-order polarizability $\langle\beta\rangle$ vales (Debye-Angstrom.$^{-1}$) of compounds with their tensors

Compounds	β_{xxx}	β_{xxy}	β_{xyy}	β_{xzz}	β_{yzz}	β_{zzz}	β_{Total}
AH1	−5.294	104.598	25.664	42.652	14.439	54.537	69.64
AH2	20.903	24.543	−271.749	−106.971	34.574	8.715	70.73
AH3	44.552	277.048	−11.289	4.775	−52.110	−7.593	40.09
AH4	314.903	256.538	−161.446	57.747	22.319	−52.262	93.12
AH5	278.361	495.686	580.474	34.551	4.047	−140.571	230.11
AH6	−84.346	672.767	69.743	7.176	−167.646	31.748	80.14
AH7	−59.457	214.866	66.468	15.218	6.629	48.510	72.52

Table 5 Natural bond orbital charge analysis between donor and acceptor groups with the role of π-linkers

Compounds	Donor	Linker	Acceptor
AH1	3.780	0.89	0.039
AH2	7.975	1.23	0.0478
AH3	3.802	1.14	0.2473
AH4	3.340	1.98	0.9810
AH5	3.300	1.98	0.8302
AH6	3.120	1.01	0.3342
AH7	5.310	2.12	0.8507

higher charge transfer capabilities has the greatest NBO values at π-conjugated linkers, whereas the **AH5** has the lowest values. All the other dyes that have been created are in good harmony with one another.

Molecular electrostatic potentials

The electrostatic potential (ESP) mapping is extremely useful for determining molecules with electrophilic and nucleophilic interaction areas. The positive (most electron-poor) component is represented in blue, while the neutral component is depicted in green, and the negative (most electron-rich) section is indicated in red (Fig. 6). Within MEP, greater negative potential zones, shown by a red color spot, are advantageous for electrophilic substitution, whereas higher positive potential zones, represented by a blue

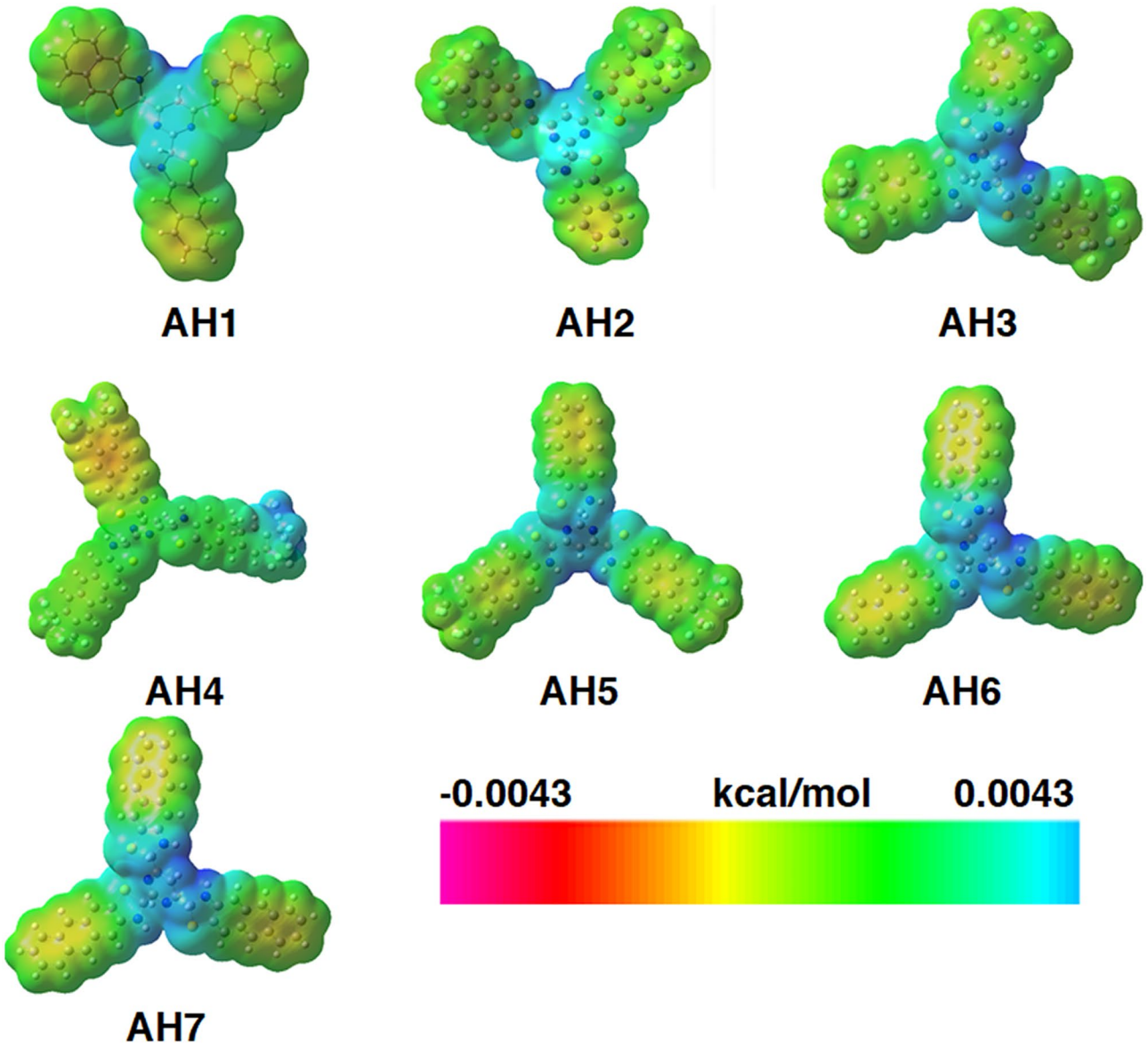

Fig. 6 Electrostatically mapped surfaces of start shaped new dyes ((**AH1**–**AH7**)

color spot, are advantageous for nucleophilic substitution approach.

Conclusions

The impact of various π-spacers on NLO characteristics was investigated when 2,2′-(pyrimidine-4,6-diyl) bis(2,3-dihydro-1,3-benzothiazole) (**PB**) chromophores (**AH1–AH7**) were hypothetically created by structural customizing with various pi-spacers. The results show that the π-linker had a promising influence on the D–π–A architecture, tuning the electrical, photo physical, and NLO characteristics of developed chromophores significantly. All the new dyes studied herein had a wider spectral response and had good **LHE** with the lowest transition energy. In **AH3**, the highest redshift ($\lambda_{max} = 436$ nm) was explored. According to the FMO investigations, HOMO was partially moved across **PB** and partially on π-linkers or acceptors (**TFM**). Most LUMOs, on the other hand, were mounted on TFMs (acceptor) and partially on phenyl π-conjugates. Furthermore, the least bandgap 0.84–3.67 eV in **AH1–AH7** was investigated. The findings of the NBO revealed that electrons are efficiently transported from PB to **TFM** via the π-linker, resulting in the formation of a charge transferring state. Electronic transitions from donor to acceptor moieties through π-conjugated linkers were shown to have a larger linear and nonlinear response. When compared to pyrrole, molecules having an imidazole spacer had a reduced bandgap and stronger NLO characteristics. Overall, all the designed compounds exhibited a strong NLO response with higher polarizability and first hyperpolarizability values, with **AH5** having the highest β_{tot} value of 230.11 Debye-Angstrom^{-1}, which was about 5 times higher than the thiazole-based identified molecules. These organic metal-free dyes based on the D–A frameworks are important in research and bring fresh insights into trials to produce high-performance NLO components.

Supplementary Information The online version contains supplementary material available at https://doi.org/10.1007/s11224-022-01983-3.

Acknowledgements The authors are grateful to the University of Management and Technology Lahore for accessing the all-research facilities. AUH and CG are also thankful to Marmara University, Istanbul, for allowing them to work on their molecular simulation lab.

Author contribution AUH: conception and design of the study; AM: resources, funding acquisition, CG: acquisition of data and drafting the manuscript. SN: editing the manuscript. SUH: read the final version of the manuscript and provided valuable discussions. MJ: revising and editing the manuscript. NNK: formal analysis.

Data availability All data generated or analyzed during this study are included in this published article and its supplementary information file.

Code availability Gaussian 09 W and Gauss view 5.1 are used for simulation and origin software is used to draw the plots.

Declarations

Ethics approval This article does not contain any studies with human participants or animals, clinical trial registration, or plant reproducibility performed by any authors.

Consent for publication All authors have approved the paper and agree with its publication.

Conflict of interest The authors declare no competing interests.

References

1. Zou G, Ok KM (2020) Novel ultraviolet (UV) nonlinear optical (NLO) materials discovered by chemical substitution-oriented design. Chem Sci 11:5404–5409
2. Chen H, Li Y-Y, Li B et al (2020) Salt-inclusion chalcogenide [Ba4Cl2][ZnGa4S10]: rational design of an IR nonlinear optical material with superior comprehensive performance derived from AgGaS2. Chem Mater 32:8012–8019
3. Manojlovic M, Cabilovski R, Bavec M (2010) Organic materials: sources of nitrogen in the organic production of lettuce. Turkish J Agric For 34:163–172
4. Hu J, Wu J, Qu X (2018) Decomposition characteristics of organic materials and their effects on labile and recalcitrant organic carbon fractions in a semi-arid soil under plastic mulch and drip irrigation. J Arid Land 10:115–128
5. Chen H-Z, Bai R, Cao L et al (2008) CNT-based organic-inorganic composite materials with optoelectronic functionality. Res Chem Intermed 34:115–125
6. Lin Y, Zhan X (2016) Oligomer molecules for efficient organic photovoltaics. Acc Chem Res 49:175–183
7. Singh J (2010) Study of organic light-emitting devices (OLEDs) with optimal emission efficiency. Phys status solidi c 7:984–987
8. Xu Y, Minari T, Tsukagoshi K et al (2011) Origin of low-frequency noise in pentacene field-effect transistors. Solid-State Electron 61:106–110
9. Wang WV, Zhang Y, Li X-Y et al (2021) High performance nonvolatile organic field-effect transistor memory devices based on pyrene diimide derivative. InfoMat 3:814–822. https://doi.org/10.1002/inf2.12186
10. Yadav S, Srivastava PK, Ghosh S (2013) Small π-conjugated organic molecules based transistor and inverter with Cu electrodes. Org Electron 14:3415–3422
11. Zhang G, Chan JMW (2017) Reversibly thermochromic bismuth-organic materials with tunable optical gaps. J Mater Chem C 5:10007–10015
12. Ogle J, Powell D, Flannery L, Whittaker-Brooks L (2021) Interplay between morphology and electronic structure in emergent organic and π-d conjugated organometal thin film materials. Ind & Eng Chem Res 60:15365–15379
13. Hassan AU, Sumrra SH (2022) Exploring the bioactive sites of new sulfonamide metal chelates for multi-drug resistance: an experimental versus theoretical design. J Inorg Organomet Polym Mater 32:513–535. https://doi.org/10.1007/s10904-021-02135-6

14. Chung H, Diao Y (2016) Polymorphism as an emerging design strategy for high-performance organic electronics. J Mater Chem C 4:3915–3933
15. Zhang X, Gui Y, Xiao H, Zhang Y (2016) Analysis of adsorption properties of typical partial discharge gases on Ni-SWCNTs using density functional theory. Appl Surf Sci 379:47–54
16. Gounden D, Nombona N, Van Zyl WE (2020) Recent advances in phthalocyanines for chemical sensor, non-linear optics (NLO) and energy storage applications. Coord Chem Rev 420:213359
17. Dudley JM, Finot C, Richardson DJ, Millot G (2007) Self-similarity in ultrafast nonlinear optics. Nat Phys 3:597–603
18. Van Erps J, Luan F, Pelusi MD et al (2010) High-resolution optical sampling of 640-Gb/s data using four-wave mixing in dispersion-engineered highly nonlinear As $ _2 $ S $ _3 $ planar waveguides. J Light Technol 28:209–215
19. Sudarsan V (2012) Optical materials: fundamentals and applications. Funct Mater. https://doi.org/10.1016/B978-0-12-385142-0.00008-8
20. Medishetty R, Zar\keba JK, Mayer D, et al (2017) Nonlinear optical properties, upconversion and lasing in metal-organic frameworks. Chem Soc Rev 46:4976–5004
21. Albrecht G, Ubl M, Kaiser S et al (2018) Comprehensive study of plasmonic materials in the visible and near-infrared: linear, refractory, and nonlinear optical properties. ACS Photonics 5:1058–1067
22. Li K, Sun M, Zhang W-D (2018) Polycyclic aromatic compounds-modified graphitic carbon nitride for efficient visible-light-driven hydrogen evolution. Carbon N Y 134:134–144
23. Koohi M, Bastami H (2020) Substituent effects on stability, MEP, NBO analysis, and reactivity of 2, 2, 9, 9-tetrahalosilacyclonona-3, 5, 7-trienylidenes, at density functional theory. Monatshefte für Chemie-Chemical Mon 151:11–23
24. Jin W, Zhang W, Tudi A et al (2021) Fluorine-driven enhancement of birefringence in the fluorooxosulfate: a deep evaluation from a joint experimental and computational study. Adv Sci 8:2003594
25. Aydın G, Koçak O, Güleryüz C, Yavuz I (2020) Structural order and charge transfer in highly strained carbon nanobelts. New J Chem 44:15769–15775. https://doi.org/10.1039/D0NJ0345
26. Ye J-T, Wang H-Q, Zhang Y, Qiu Y-Q (2019) Regulation of the molecular architectures on second-order nonlinear optical response and thermally activated delayed fluorescence property: homoconjugation and twisted donor-acceptor. J Phys Chem C 124:921–931. https://doi.org/10.1021/acs.jpcc.9b10067
27. Hassan AU, Mohyuddin A, Nadeem S et al (2022) Structural and electronic (Absorption and Fluorescence) aroperties of a stable triplet diphenylcarbene: a DFT study. J Fluoresc. https://doi.org/10.1007/s10895-022-02969-4
28. Hassan AU, Sumrra SH, Zafar MN et al (2021) New organosulfur metallic compounds as potent drugs: synthesis, molecular modelling, spectral, antimicrobial, drug-likeness and DFT analysis. Mol Divers. https://doi.org/10.1007/s11030-020-10157-4
29. Dufresne S, Hanan GS, Skene WG (2007) Preparation, photophysics, and electrochemistry of segmented comonomers consisting of thiophene and pyrimidine units: new monomers for hybrid copolymers. J Phys Chem B 111:11407–11418. https://doi.org/10.1021/jp075259j
30. Lee C, Yang W, Parr RG (1988) Development of the Colle-Salvetti correlation-energy formula into a functional of the electron density. Phys Rev B 37:785–789. https://doi.org/10.1103/PhysRevB.37.785
31. Legler CR, Brown NR, Dunbar RA et al (2015) Scaled quantum mechanical scale factors for vibrational calculations using alternate polarized and augmented basis sets with the B3LYP density functional calculation model. Spectrochim Acta Part A Mol Biomol Spectrosc 145:15–24
32. Sumrra SH, Hassan AU, Zafar MN et al (2022) Metal incorporated sulfonamides as promising multidrug targets: combined enzyme inhibitory, antimicrobial, antioxidant and theoretical exploration. J Mol Struct 1250:131710. https://doi.org/10.1016/j.molstruc.2021.131710
33. Hassan AU, Sumrra SH, Imran M, Chohan ZH (2022) New 3d multifunctional metal chelates of sulfonamide: spectral, vibrational, molecular modeling, DFT, medicinal and in silico studies. J Mol Struct 132305. https://doi.org/10.1016/j.molstruc.2021.132305
34. Hlel A, Mabrouk A, Chemek M et al (2015) A DFT study of charge-transfer and optoelectronic properties of some new materials involving carbazole units. Comput Condens Matter 3:30–40
35. Shengelaya A, Zhao G, Keller H, Müller KA (1996) EPR evidence of Jahn-Teller polaron formation in La 1–x Ca x MnO 3+ y. Phys Rev Lett 77:5296
36. Saha SK, Hens A, Murmu NC, Banerjee P (2016) A comparative density functional theory and molecular dynamics simulation studies of the corrosion inhibitory action of two novel N-heterocyclic organic compounds along with a few others over steel surface. J Mol Liq 215:486–495
37. Gun'Ko VM, Zarko VI, Goncharuk E V, et al (2007) TSDC spectroscopy of relaxational and interfacial phenomena. Adv Colloid Interface Sci 131:1–89
38. Torre MH, Gambino D, Araujo J et al (2005) Novel Cu (II) quinoxaline N 1, N 4 -dioxide complexes as selective hypoxic cytotoxins. 40:473–480. https://doi.org/10.1016/j.ejmech.2004.11.012
39. Huber MCE, Sandeman RJ (1986) The measurement of oscillator strengths. Reports Prog Phys 49:397
40. Meyers F, Marder SR, Pierce BM, Bredas J-L (1994) Electric field modulated nonlinear optical properties of donor-acceptor polyenes: sum-over-states investigation of the relationship between molecular polarizabilities (. alpha., beta., and. gamma.) and bond length alternation. J Am Chem Soc 116:10703–10714
41. Henari FZ, Morgenstern K, Blau WJ et al (1995) Third-order optical nonlinearity and all-optical switching in porous silicon. Appl Phys Lett 67:323–325
42. Kvalheim MD, Revzen S (2021) Existence and uniqueness of global Koopman eigenfunctions for stable fixed points and periodic orbits. Phys D Nonlinear Phenom 132959
43. Glendening ED, Landis CR, Weinhold F (2012) Natural bond orbital methods. Wiley Interdiscip Rev Comput Mol Sci 2:1–42. https://doi.org/10.1002/wcms.51
44. Quiroz-Garc\'\ia B, Figueroa R, Cogordan JA, Delgado G, (2005) Photocyclodimers from Z-ligustilide. Experimental results and FMO analysis. Tetrahedron Lett 46:3003–3006
45. Sumrra SH, Arshad Z, Zafar W et al (2021) Metal incorporated aminothiazole-derived compounds: synthesis, density function theory analysis, in vitro antibacterial and antioxidant evaluation. R Soc Open Sci 8:210910
46. Omidvar A (2017) Electronic structure tuning and bandgap opening of nitrogen and boron-doped holey graphene flake: the role of single/dual doping. Mater Chem Phys 202:258–265
47. Anguile JJ, Ngnabeuye ON, Bridget NN et al (2018) Synthesis, characterization and DFT studies of two zinc(II) complexes based on 2-isopropylimidazole. Open J Inorg Chem 08:105–124. https://doi.org/10.4236/ojic.2018.84009
48. Hassan AU, Sumrra SH, Raza MA et al (2021) Design, facile synthesis, spectroscopic characterization, and medicinal probing of metal-based new sulfonamide drugs: a theoretical and spectral study. Appl Organomet Chem n/a:e6054. https://doi.org/10.1002/aoc.6054
49. Tachibana Y, Hara K, Sayama K, Arakawa H (2002) Quantitative analysis of light-harvesting efficiency and electron-transfer yield in ruthenium-dye-sensitized nanocrystalline TiO2 solar cells. Chem Mater 14:2527–2535

50. Imahori H (2004) Giant multi porphyrin arrays as artificial light-harvesting antennas. J Phys Chem B 108:6130–6143
51. Liyanage PS, de Silva RM, de Silva KMN (2003) Nonlinear optical (NLO) properties of novel organometallic complexes: high accuracy density functional theory (DFT) calculations. J Mol Struct THEOCHEM 639:195–201
52. Oudar J-L, Chemla DS (1977) Hyperpolarizabilities of the nitro aniline and their relations to the excited state dipole moment. J Chem Phys 66:2664–2668
53. Del Freo L, Terenziani F, Painelli A (2001) Static NLO susceptibilities: testing approximation schemes against exact results. arXiv Prepr physics/0106084
54. Piper LG, Cowles LM (1986) Einstein coefficients and transition moment variation for the NO (A 2$Σ$+–X 2$Π$) transition. J Chem Phys 85:2419–2422
55. Di Bella S, Fragala IL, Ratner MA, Marks TJ (1993) Electron donor-acceptor complexes as potential high-efficiency second-order nonlinear optical materials. A computational investigation. J Am Chem Soc 115:682–686
56. Raposo MMM, Fonseca AMC, Castro MCR et al (2011) Synthesis and characterization of novel diazenes bearing pyrrole, thiophene and thiazole heterocycles as efficient photochromic and nonlinear optical (NLO) materials. Dye Pigment 91:62–73
57. Breitung EM, Shu C-F, McMahon RJ (2000) Thiazole and thiophene analogues of donor-acceptor stilbenes: molecular hyperpolarizabilities and structure-property relationships. J Am Chem Soc 122:1154–1160
58. Muhammad S, Kumar S, Koh J et al (2018) Synthesis, characterisation, optical and nonlinear optical properties of thiazole and benzothiazole derivatives: a dual approach. Mol Simul 44:1191–1199
59. El-Shishtawy RM, Borbone F, Al-Amshany ZM et al (2013) Thiazole azo dyes with lateral donor branch: Synthesis, structure and second-order NLO properties. Dye Pigment 96:45–51
60. Sumrra SH, Hassan AU, Imran M et al (2020) Synthesis, characterization, and biological screening of metal complexes of novel sulfonamide derivatives: Experimental and theoretical analysis of sulfonamide crystal. Appl Organomet Chem. https://doi.org/10.1002/aoc.5623
61. Hassan AU, Guleryuz C (2021) Theoretical evaluation of the permeability of discharge item (LiOOH) in Li-O-2 batteries. Lat Am Appl Res 51:153–157